CORPUS PUBLISHERS

Journal of Mineral and Material Science (JMMS)

Volume 3 Issue 2, 2022

Article Information

Received date : May 14, 2022

Published date: June 22 2022

*Corresponding author

Inyiama Fidelis Chidozie, Department of Chemical Engineering, Enugu State University of Science and Technology, Enugu, Nigeria

Keywords

Charaterization; Application; Kaolinite; Formulation; Porcelain; Manufacture

Research Article

Characterization and Application of Nigerian Clay Raw Resources for Porcelain Formulation and Manufacture

Chidozie IF* and Thompson CO

Department of Chemical Engineering, Enugu State University of Science and Technology, Enugu, Nigeria

Abstract

Porcelain is a ceramic material made by heating refined minerals (clay) in the form of kaolinite to high temperature in a kiln at temperatures between 1200 °C – 1400 °C thus converting ceramic body irreversibly to hard product, impermeable to water and chemicals. The use of three minerals (kaolin, feldspar and sand) from Nigeria in the formulation and production of porcelain has been investigated in this study, with kaolin bond in the formulation intended to increase the thermal strength of the product. Characterization results showed that the clay contains kaolinite (58%), quartz (15%), rutile (0.5%) and illite (15%). Sample was formulated and shaped by casting into molds and sintered at temperatures ranging from 1200 °C – 1300 °C. Characterization of porcelain specimen sintered at 1250oC showed interesting results: a density ranging from 2.16-2.25g/cm^3; open porosity of less than 1.03%; flexural strength above 50MPa and water absorption below 0.5%.

Introduction

The term "clay" is a naturally occurring material primarily made of fine-grained minerals (clay minerals), being generally plastic at appropriate water contents and hardening when dried or fired with particle size of less than 2 µm. These materials are layered structures mainly composed of SiO_4 tetrahedral sheets linked by oxygen atoms to XO_6 octahedral sheets (X=Al, Fe, Mg). According to their layered structure, clay minerals are classified in seven groups: kaolin-serpentine, pyrophyllite-talc, smectite, vermiculite, mica, chlorite and interstratified clay minerals [1]. The clay minerals structure and chemical composition determine its corresponding application. Natural clay minerals contain impurities and are not homogenous, which cause their use to be difficult for technological applications. Therefore, in order to improve their properties, it is necessary to prepare mixtures to enhance them with the use of additives. Some of the relevant properties for porcelain production have to do with color and brightness, which ultimately depend on the clay's mineral content and the firing temperature it is subjected to. This means that adequate characterization of raw materials and control of firing process is key for technological processes in the manufacture of porcelain. Kaolin clay which is a primary component in porcelain is referred to as china clay, comprise predominately the mineral kaolinite ($Al_2 Si_2O_5(OH)_4$), a hydrous aluminium silicate, and small quantity of various impurities, such as quartz, micas, smectite, graphite, iron oxides, iron sulphides and/or titanium-based impurities [2]. Kaolin is generally known as a white inorganic pigment existing naturally and beneficiated as kaolin clay. Porcelain building materials and laboratory equipment widely used in secondary, tertiary institutions and industries such bricks, floor tiles, stoneware tiles, porcelain boats, vacuum filters, milling balls, porcelain funnels, jars, beakers, crucibles, combustion boats, Petri dish, desiccators plate, dental dissolving cups, pipette rest, round capsules, bullet proof ceramics etc. are produced from this natural occurring clay mineral and its additives [3,4]. The objective of this study is to contribute to the potential use of mineral resources from Nigeria in porcelain composition. The mass loss and shrinkage of different formulations were measured by using Differential Thermal Analysis (DTA). Physico-chemical and mineralogical characteristics of the porcelain samples were investigated and the experiments led to the measurement of bulk density, linear shrinkage, water absorption, strength and total porosity. Porcelain is formulated from a typical triaxial mixture usually involving 25wt.% kaolin, 25wt.% silica and 50wt.% feldspar (generally sodium feldspar) for soft porcelain and 50wt.% kaolin clay, 20wt.% silica and 30wt.% feldspar (generally potassium feldspar) for hard porcelain [4-7]. The kaolin clay fraction shape and provide plasticity and dry mechanical strength during processing. In the firing process kaolin clay has a role in mulite recrystallization and in the formation of a vitreous phase. Feldspar contributes in the quantity and behaviour of the liquid phase at temperature above 1050 °C. It contributes to control the sintering process, allowing a virtually zero (< 0.5%) open porosity and low level of closed porosity (<10%). The quartz is used as filler to promoted thermal and dimensional stability due to its high melting point and is involved in recrystallization processes and in liquid phase behaviour [5,8,9].

Materials and Methods

Materials

Table 1: Summary of raw materials location in Nigeria.

S/N	Name	State	L.G.A	Location
1	Feldspar	Kogi	Adavi	Aku, Zariaji, Asara
2	Silica Sand	Anambra	Yagba West Lokoja Anyamelu	Isanlu East Lokoja Igbariam
			Aguata South Anambra East	Nkpologwu Otuocha
3	Glass Sand	Enugu Enugu	Udi Enugu North Udi	Nsude Iva Valley Nsude
4	Kaolin	Plateau	Nsukka Barkin Ladi Riyon	Agu Opi Major Porter Werram
		Ogun	Bokkos Abeokuta North	Pykaru, Metzet Abeokuta
			Yewa North	Aiyetoro
			Ijebu Ode Imeko/ Afon	Ijebu Ode Imeko
5	Tin-Oxide (Columbite)	Plateau	Pantshin Mangu Bokkos	Wasisf, (Futuk) Gaude, Kantoma, Yidel Pykalu, Anancha
6	Talc	Bauchi Niger	Ningi Rafia	Jigawa Abuchi, Kangara, Kamunu
7	Gypsum	Enugu	Uzo Uwani	Adani
		Benue	Igboeze North Okpogwu	Igga Edumaga
		Gombe	Otukpo Bidiri	Umogidi Lakata
			Nafada	Baruwa
		Yobe	Fika	Fika (Fune/Manawaji), Manjij, A

The raw mineral used in this study was obtained from an open pit from the summary of raw material locations in Nigeria Table 1 below. In this study, raw kaolin slurry was generated by washing the grained graphite of Agu-Opi clay 10kg lumps which was crushed, ground and washed with a high-pressure water jet. The coarser grain and heavier sand, mica, feldspar and other associated minerals were removed using a variety of processes combining gravity settling, mechanical separation and hydro-cyclone to collect kaolinite-rich clay slurry less than (< 100μm) fraction which consists mostly of kaolinite particle. All powders of the composite triaxial mineral were screened below 100μm. The fine powders were then mixed according the designed formulation.

Experimental methods

Youssouf et al. [5] method was adapted for the experimental methods. The mineralogical composition was obtained with a diffractometer (Philips PW 1710, France) in step scan mode using N-filtered CuKa radiation (1.5406A); wide range x-ray spectra were recorded with a D500. Elemental chemical analysis were performed by Induced Coupled Plasma (ICP), Iris, marketed by Thermo Jorrell (Cheshire, England). The thermal analyses have been recorded for both Differential Thermal Analysis (DTA) and Thermogravimetry (TG) anaysis. It was obtained with a SETARAM Setsys 24 using Pt crucibles, and a heating rate of 10 °C/min. Experiments were carried out with 50mg of powder into the crucible and a pure α alumina calcined powder at 1500 °C serves as a reference material in adequate quantity to reduce the calorimeter imbalance. The kiln atmosphere was air at atmospheric pressure. The sintering behaviour of sample was characterized by dilatometry versus temperature (horizontal push rood dilatometer ADAMEL DI. The length of small cylindrical bar (3x3x15mm) was measured during controlled thermal cycles under flowing air. The temperature ramp was 10 °Cmin^{-1}. Chemical analyses of the samples were carried out by X-ray fluorescence and the loss of ignition was obtained with a Nabertherm 250C type furnace at 1000 °C. The semi-quantification of the identified minerals phases presented in the sample was calculated with the method described by [10]. The raw materials were first finely crushed and sieved to a particle size ϕ < 46μm. A formulation blend of 50wt% kaolin, 30wt% feldspar and 20wt % quartz was prepared. Water was added in a weight ratio 1/2 (water/mixture). Sodium carbonate (0.75wt %) was added to promote the repulsive forces creating an electrostatic network which prevents the agglomeration of the particles and facilitates their mobility in aqueous mixtures. Mixtures were homogenized in a roller jar placed on a rotary mixer at a speed of 75 revolutions per minute for a period of 10min. The liquid mixture was subsequently poured into porous plaster molds to shape tile samples (50x50x8mm).Tile sample demolding was after 15min of water absorption by plaster. After demolding, the samples were preliminary dried in air for 24h, and subsequently in a laboratory dryer at 80 °C. Firing of dry samples in an electric kiln was at a heating rate of 10 °C/min up to the temperatures of 1200 °C, 1220 °C, 1250 °C, 1280 °C and 1300 °C). At maximum firing temperature, a dwell of 1h is applied before cooling down at a rate of 10 °C/min.

Linear Shrinkage (LS) was evaluated by the relative variation of length (L_s the initial length and L_c the final length) of the tiles using a calliper Equ.1, [5,11].

$$L_S = \frac{L_S - L_C}{L_S} \times 100 \quad (1)$$

where L_s and L_c represent the dimensions (mm) of the green and fired specimens respectively. The water absorption (WA(%),), bulk density and apparent porosity were measured according to ASTM C373-88, which involves drying the test specimens to constant mass (D), boiling in distilled water for 5h and soak for an additional 24h at ambient temperature. After impregnation, the mass (S) of each specimen while suspended in water and their saturated mass (M) is determined. The test was carried out on four representative specimens. The difference in mass gives the mass of water absorbed by the specimen during this time. The water absorption is evaluated according to Equ.(2): Water absorption, WA(%), expresses the relationship of the mass of water absorbed to the mass of the dry specimen.

$$W_A\% = \frac{M - D}{D} \times 100 \quad (2)$$

The bulk density was determined using Equations (3) and (4). The test consists in successively measuring the mass and the volume of the sample. The volume is deduced from three weighing, one of which is made after immersing the sample in water (m) and waxed immediately afterwards in paraffin (m_p) in the open air, and then placed in a basket suspended from the stirrup and immersed in order to be weighed hydrostatically m_p.

$$\rho = m/\upsilon \quad (3)$$

With

$$v = \frac{m_p - m_p}{\rho_W} - \frac{m_p - m}{\rho_p} \quad (4)$$

where under the same conditions of temperature and pressure: ρ_w is the density of water (1000 kg/m^3); ρ_p is the density of paraffin (880kg/m^3); m the mass of the sample; m_p the mass of the paraffinic sample and m_p the hydrostatic mass of the waxed sample.

Flexural mechanical properties are obtained by three-point flexural tests with rectangular cross-section specimens. They were placed on two parallel supporting pins and the loading force is applied in the middle by means of a loading pin. The supporting and loading pins are mounted in a way to allow their free rotation about the axis parallel to the pin axis. This configuration provides uniform loading of the specimen and prevents friction between the specimen and the supporting pins, [12-14]. The fracture strength was obtained with samples having a width of B=9mm and a thickness of W=6–8mm. The 3-point bending device had a span L=40mm. The testing apparatus was an Instron type, equipped with a load cell of 10kN and the Bluehill 2 software. The crosshead speed was 1mm/min. The maximum load at failure (Fr) was converted into fracture strength (σ_r) using the usual relation equation (5) that is valid for rectangular samples.

$$\sigma_r = \frac{3}{2}\frac{LF_r}{BW^2} \quad (5)$$

Results

Chemical analysis of raw materials

The chemical composition of the raw material used is shown in Table 2. Data indicate that the clay and feldspar are alumina-silicates. For the ratio SiO_2/Al_2O_3 (approximately 2.13) is higher than that of pure kaolinite (approximately 1.18) from the presence of free silica, [15,16]. The relatively high content of potassium oxide (% K_2O=2.22) suggests the presence of micaceous phases (muscovite or illite). For a fairly high alkaline oxides content (%K_2O+% Na_2O=3.54) suggests the predominance of mixed feldspar minerals and mica phases. The strong predominance of silica results from quartz [17].

Table 2: Chemical and mineralogical analysis of clay materials of Agu-opi clay.

% Composition	Kaolin (wt%)	Feldspar (wt%)	Sand (wt%)
SiO_2 (%)	66.6	43.2	90.42
TiO_2 (%)	0.37	0.28	0.84
Al_2O_3 (%)	31.2	18.81	2.45
Fe_2O_3 (%)	1.53	0.86	0.58
Pb (%)	0.25	0.07	0.35
CaO (%)	0.66	0.62	0.12
MgO (%)	1.37	0.4	0.03
K_2O (%)	2.22	11.3	0.62
Na_2O (%)	1.32	1.94	0.04
MnO (%)	0.04	-	0.008
LOI (%)	6.08	0.50	0.6
Surface area (m^2/g)	8.17	5.6	0.85
Brightness (%)	56.8	48.3	-
Brownish-red	10.5	12.3	-
< 53μm (%)	0.1	0.02	0.05
< 10μm (%)	10	7	15
< 2μm (%)	46	23	34

Mineralogical characterization of raw materials

XRD analysis was carried out to determine the mineralogical compositions. The result show that the sample contains mainly kaolinite phase ($Al_2Si_2O_5(OH)_4$), halloysite as a secondary phase in small quantities illite ($(K, H_3O)Al_2Si_3AlO_{10}(OH)_2$) and rutile($Ti_2O_3$). The identified mineralogical compositions of the raw materials with their chemical analyses validate our primary assumption that porcelain compositions can be obtained from Nigerian local mineral materials (Table 1 & Figure 1). These results deduced from elementary chemical analysis, showed that the kaolin contains small quantity of impurities such as Fe_2O_3, K_2O, CaO and MnO, which is consistent with the white kaolin clay. The proportion of Si2O in the feldspar 43.2 wt.% can contribute to the formulation of the liquid phase. The percentage of SiO_2 in the quartz above 80 wt.% according to, Garcia and Angular-Elguezaba [18] and the results obtained of raw material used are alumino-silicate materials. Besides, it is important to note the iron oxide content of the samples 1.5 for their use in porcelain production was beneficiated to avoid the black core and changes on col-orimetric properties. Fe_2O_3 content above 0.04 wt.% will negatively impact on the whiteness and refractiveness of porcelain product as little coloration is magnified by the firing process. The mineral material yielded a preferred orientation of kaolin pattern with all peaks clearly resolved. The peaks at approximately 2θ=12, 17, 20, 22, 25, 27, 35, 37° confirms kaolinite while those at 2θ=8, 17, 30 and 45 correspond to illite.

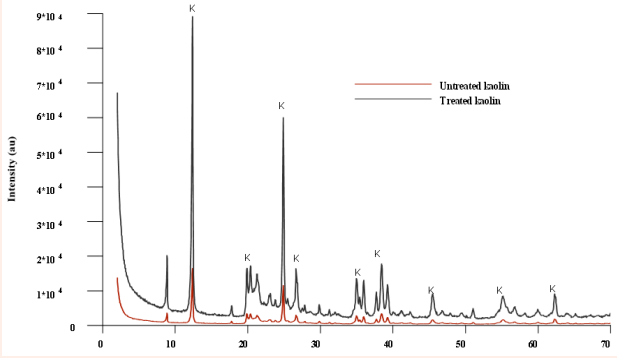

Figure 1: XRD patterns of kaolin before and after its bioleaching.

Formulation of the triaxial composite

In order to build all ternary plots, a mixture design, Ayadi et al. [19] with 13 experiments were selected, as shown in Table 3 and Figure 2. Considering that the measurements for ternary plots containing the high viscosity kaolin were carried out with 60vol.% kaolin, 20vol.% feldspar and 20vol.% quartz sand respectively and the fact that some vertices and edges were common to some triple mixture ternary diagrams, a total of 30 rheology measurements were made. The density of the samples was determined using pycnometry. Humidity tests were performed to determine moisture contents and the exact quantity of mineral and water to be added when preparing the slurries and the briquettes. The same mixture design using spectral features mathematical models have been developed, not contained in this report, for detecting the presence of any of the three minerals, and once detected, another model was applied towards estimating the abundance (volumetric fraction) of that specific mineral in a sample, leading to a point on a ternary plot for viscosity and another for yield stress obtained from a fitted Bingham Plastic Model, Kwak et al. [20]. From the result of the ternary plot diagram, composition formulation within envelop-A gives hard paste formation that do not slump in the kiln under high temperature firing, while composition formulation within envelop-B gives soft paste formulation that slumps in the kiln under high temperature firing. The point marked red in the ternary diagram gives the best formulation of 50 vol.%.kaolin, 30 vol.%.feldspar and 20 vol.%.sand for ease of workability and manipulation. This formulation from the local clay is in substantial conformity to 40-50 vol.% kaolin clays, 35-45 vol.% feldspars and 10-15 vol.% quartz sand proposed by Martin-Marquez [16,21] as typical composition for commercial porcelain. The presence of quartz in the ceramic body may be considered beneficial as it facilitates the excretion of gaseous materials in the firing stages, decreases the drying shrinkage, and improves the whiteness of the final product. However, high quartz content causes a reduction in the plasticity and strength of the unfired material, abrasion of the operational equipment, and health threats [22].

Table 3: Mixture design for each ternary plot, A, B and C being any three minerals from the selected (kaolin, Feldspar and silics sand) composite used.

Mineral A (Vol.%) Kaolin	Mineral B (Vol.%) Feldspar	Mineral C (Vol.%) Silica	Total (Vol. %)
100			100
67.7		33.3	100
33.3		67.7	100
	100		100
60	20	20	100
20	20	60	100
67.7	33.3		100
33.3	33.3	33.3	100
	33.3	67.7	100
33.3	67.7		100
20	60	20	100
67.7	33.3		100
		100	100

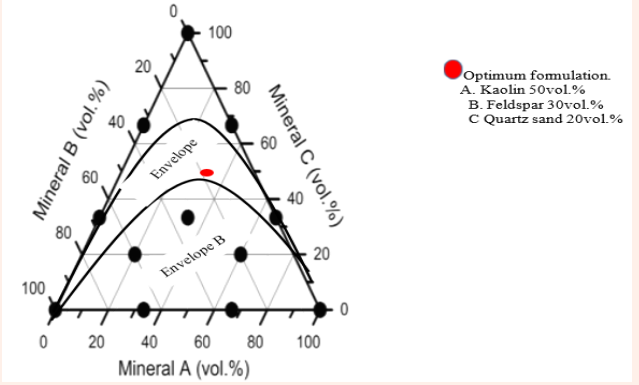

Figure 2: Mixture design over ternary plot.

Differential thermal analysis (DTA) and thermogrametry (TG)

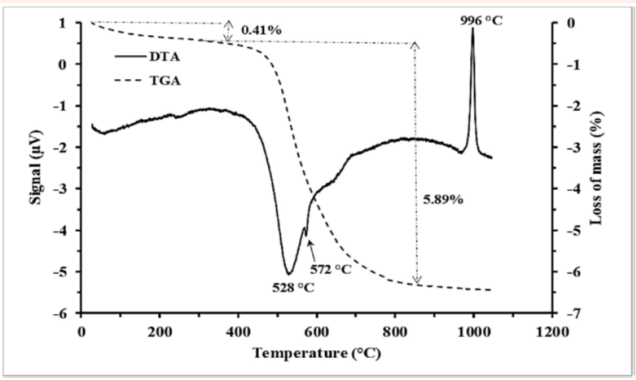

Figure 3: Thermograms DTA/TG of porcelain.

The thermograms of samples (Figures 3 & 4) were carried out at a heating rate of 10 °C/min under air atmosphere, using a SETARAM Setsys equipment. Weights of samples and of the reference alumina are 50mg inside identical platinum crucibles. The thermal analysis (Figure 3) showed that from room temperature to 225 °C, endothermic peaks in the DTA curve is accompanied with a 0.41% loss of mass in TG curve. This endothermic reaction is related to the escape of interlayer water of mineral phases [23]. The endothermic peaks at 528 °C is more accentuated and extended from 400 to 600

°C. It is correlated to a significant mass loss that is due to the loss of structural water in phyllosilicates. It is the dihydroxylation of structural OH--- in kaolinite and in illite structures, according to equation (6).

$$2(OH) \rightarrow H_2O + O_r \quad \text{(r. residual)} \quad (6)$$

In this temperature range, the breakdown of kaolinite structure leads to the formation of a quasi-amorphous material of metakaolinite [5,24,25], according to equation (7):

$$Al_2Si_2O_5(OH)_4 \rightarrow Al_2Si_2O_7 + 2H_2O \quad (7)$$

A small and sharp endothermic peak at 573 °C is not associated with a mass loss. It is related to the allotropic transformation of α-quartz to β-quartz [26]. The only occurring exothermic peak is at 996 °C, and it is not accompanied by a mass loss in the TG curve. It is from the onset of the structural reorganization process of metakaolinite, leading to the very progressive recrystallization of new phases. The sequence of transformation processes of sample occurs in agreement with some published results. They all concluded in a first step of kaolinitic structural transformation into metakaolinite below 600 °C [27,28]. In a second transformation step above about 950 °C, the metakaolinite structure undergoes a structural reorganization. The SiO_4 structural units are associated with the AlO_6 structural units to form a new spinel phase that is a precursor for the progressive formation of the mullite phase. Considering the composition of the sample, this structural reorganization occurs at a relatively high temperature (above 950 oC), that is most probably due to the relatively high crystallization degree of kaolinite in sample. The thermogram of sample Figure 4 shows a mass loss of about 0.3% at low temperature (<300 oC). It is associated with small endothermic variation that can be attributed to the interrelated or absorbed water on the surfaces of present phases. Between 400 oC and 900 oC, the DTA shows a large asymmetric peak corresponding to the dehydroxylation of muscovite [29]. The progressive mass loss associated with this transformation is about 1.5%. During dehydroxylation, the muscovite structure is progressively transformed into a high temperature form that has a low structural organization degree [30]. It follows equation (5).

$$(Si_3AlO_{10})Al_2(OH)_2K \rightarrow (Si_3AlO_{11})Al_2K + H_2O \quad (5)$$

(muscovite) (dehydrozyled muscovite)

At 565 oC, an endothermic and low intensity phenomenon has an effect in the thermogravimetric curve. It corresponds to the allotropic transformation of α-quartz to β-quartz [26]. At about 900 °C, the exothermic expansion of DTA thermogram corresponds to the recrystallization of the high temperature form of muscovite and formation of new phases. According to the ternary diagram SiO_2– $Al_2O_3K_2O$ [31], the crystallized phases are mullite and leucite (Figure 4).

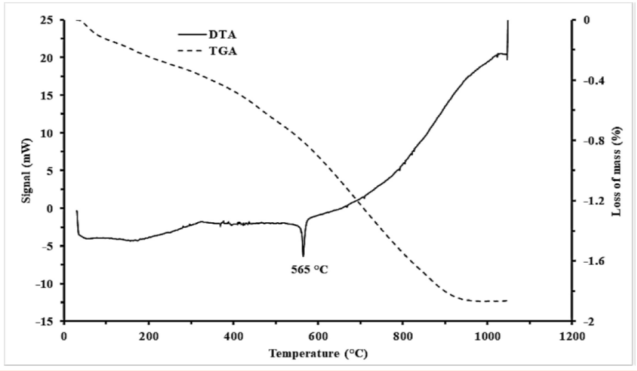

Figure 4: Thermograms DTA/TG of porcelain.

Dilatometric analysis

The dilatogram of porcelain (Figure 5) between 25 °C and 120 °C shows a first shrinkage of 0.09%. It corresponds to the dehydration of the clay [32]. The slight expansion occurring between 120 °C and 450 °C is assigned to thermal expansion of the powder compact. A second shrinkage of 0.19% is observed from 450 °C to 550 °C. This shrinkage is due to the dehydroxylation of clay minerals such as kaolinite and illite. The thermal expansion that is observed from 550 °C to 952 °C is followed by another small shrinkage of 0.42% occurring between 952 °C and 1000 °C. The latter is related to the exothermic phenomenon from the structural reorganization process of metakaolinite. Above 1000 °C, the densification process of porcelain occurs, with shrinkage of 1.34%. The dilatogram of porcelain (Figure 6) indicates an expansion in the temperature range 500 °C – 955 °C, that is related to the thermal expansion of mineral phases in the powder compact. It can be attributed to the thermal transformations of muscovite and albite minerals [33]. The progressive expansion is changed with a sharp peak at 573 °C that is associated with the allotropic transformation of quartz. Above 1000 °C, we observe the densification of the powder compact resulting in length reduction of 1.34%. It is related to a progressive liquid phase sintering process. During cooling, a step is observed during cooling at 573 °C, from the reversible quartz transformation. The porcelain sample composed of quartz present a rapid variation at 578 °C from quartz. Above that temperature, the dilatation coefficient increases. It is attributable to the existing mica phase, because the dilatation coefficient of β quartz is very small. All dilatometric curves are well correlated with DTA/TA curves since the occurrence of similar transformation temperatures.

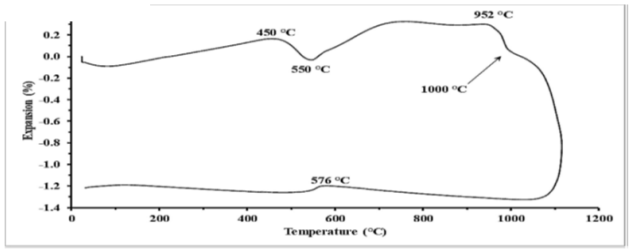

Figure 5: Dilatometric curve of porcelain.

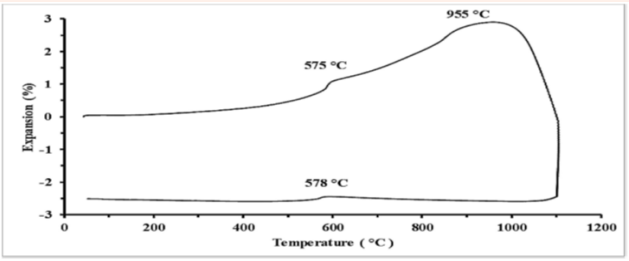

Figure 6: Dilatometric curve of porcelain.

Charaterization of the porcelain specimen

Linear shrinkage, water absorption, porosity and specimen density: Both green powder and fired samples were characterized by means of differential thermal analysis. The body shows a good sintering behavior. The fired samples are homogeneous and free of defects such as holes, bubbles or cracks. Figure 7 shows the open, close and total porosity as function of firing temperature at the 1200 °C-1350 °C range. Upon firing, these properties show the typical trend of a ceramic body sintered by a viscous liquid phase mechanism in accordance with the result of [34,35]. In fact, it is apparent that open porosity decreases with increasing firing temperature due to the formation of a glassy phase that is mainly originated from the feldspar. Increasing temperatures cause both an increase in liquid phase level and a decrease in liquid phase viscosity. Under the surface energy forces created by the fine pores contained in the ceramic body, the liquid phase tends to approach the particles and, therefore, open porosity decreases. Simultaneously, closed porosity increases in the whole firing temperature range, being this increasing considerable above 1230 °C because of the so-called body bloating due to the pressure of the gas inside the closed pores, which tends to expand the pores in line with the result of Orts et al. [36,37]. The sintering behaviour of the fired samples were evaluated by linear shrinkage, water absorption and porosity measurements. The combination of both open and closed porosity gives rise to the total porosity decrease in the first steps of sintering, reaching a minimum value at 1230 °C and then increasing. This behaviour is similar to that shown by almost all porcelain bodies. Open porosity consists of fine, interconnected pores with irregular shape. On the other hand, closed porosity is due to larger, isolated and spherical pores. The size of closed pores increases with firing temperature, from an average diameter of ~5μm at 1200 °C to 100μm at 1300 °C not shown in this report.

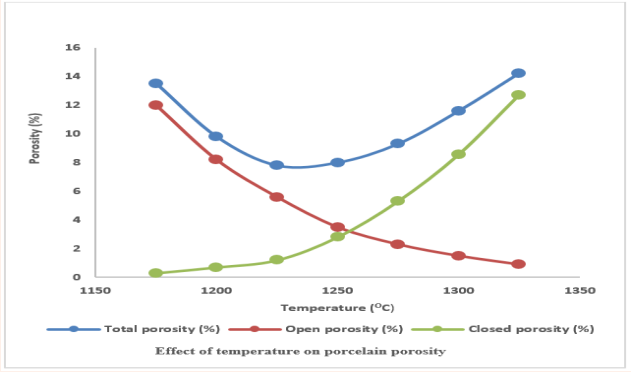

Figure 7: Total porosity (.) Open (.), close (.) of the porcelain samples as function of firing.

It is necessary to point out that the sintering process in porcelain samples does not exactly proceed by the foreseen way of a liquid phase mechanism. Kingery [37] establishes two different steps during sintering. The first shows a decrease in open porosity, which is coincident with an increase in the sample shrinkage. The sintering process is not finished when open porosity completely disappears. In the second steps, the ceramic body could be represented as a conjunction of small and closed pores. The surface energy force inside each pore give rise to a negative pressure, which tends to densify the ceramic body. However, Figures 7 show that in the porcelain samples, the closed porosity starts to increase before open porosity totally disappears. This behavior is due to both mullite crystallization and quartz dissolution in the liquid phase, which originate an increase in the viscosity of liquid phase and hence, the removal of open porosity is delayed. To discuss the degree of densification, bulk density rather than absolute density must be compared, because the content of crystalline phases affects absolute density. It has been observed that bulk density has a similar behavior to linear shrinkage; an initial increase is followed by an abrupt decrease in the relative density because of the so-called bloating according to Maity and Sarkar (34) & Amoros et al. [38]. The optimum vitrification range is achieved when open porosity reaches a minimum value, tending to be nearly zero, and simultaneously linear shrinkage is maximum value. Firing above vitrification range results in a drastic fall of the physical properties due to forced expulsion of the entrapped gases, resulting in blisters and bloating. From Figures 7, it can be established that in this porcelain paste the optimum firing temperature in the 1230 °C – 1250 °C range was achieved as the maximum firing temperature where the total porosity was minimum.

Mechanical strength of porcelain

In this study, mechanical strength, firing shrinkage (%), bulk density, total porosity (%) and elastic modulus values of samples were used to prepare calibration curves for strength analysis thus: (elastic modulus -strength , elastic modulus - total porosity, elastic modulus - bulk density, elastic modulus –firing shrinkage (Figures 8a-8d). Bulk density-ultrasonic velocity plots are commonly-used to predict the bulk density of green ceramic [39,40]. The results show that elastic modulus values are increased by increasing the strength polynomial (Figure 8a). The strength is greatly controlled by its microstructure and the presence of defects. A second important factor controlling strength is the pore fraction [41]. Depending on sintering temperature and heating rate combination, the strength increased due to a decrease of total porosity (%). Density is also a property dependent on the level of porosity. The changes reflect the counter effects of sintering reducing porosity and increasing density forming more glass phase from crystalline phases and a resultant reduction in density and increased porosity [42]. Linear shrinkage depicts a similar trend where density which initially increases reaches a maximum value and where above this value it decreases due to increasing close porosity [16]. Whereas the elastic modulus decreases with an increment of total porosity (Figure 8b), it increases with bulk density (Figure 8c) and firing shrinkage (Figure 8d).

Sintering porcelain tiles at an optimum combination of sintering temperatures and heating rates is important in order to achieve high strength, bulk density and total shrinkage, and low total porosity properties. It has been determined that sintering porcelain at 1210 °C is not sufficient to obtain optimized properties and also that 1230 °C is a temperature which results in bloating under the undertaken experimental conditions. Heating rate is most effective for sintering porcelain tiles at 1220 °C, but it has vigorous results on properties for 1210 °C and 1230 °C. In this study, sintering porcelain tiles at 1220 °C for all heating rates inspected is necessary to obtain the best properties. The results indicate that when the elastic modulus increases, the strength, firing shrinkage, bulk density also increases, but total porosity decreases. The results of the study demonstrate that a measurement of elastic modulus is a reliable tool for the characterization of strength, firing shrinkage, bulk density and total porosity in porcelain.

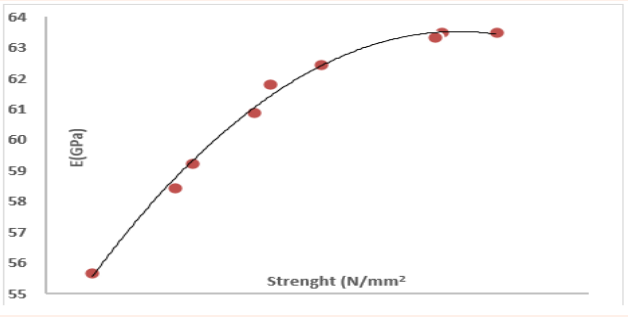

Figure 8a: The relationship between elastic modulus (E values and strength).

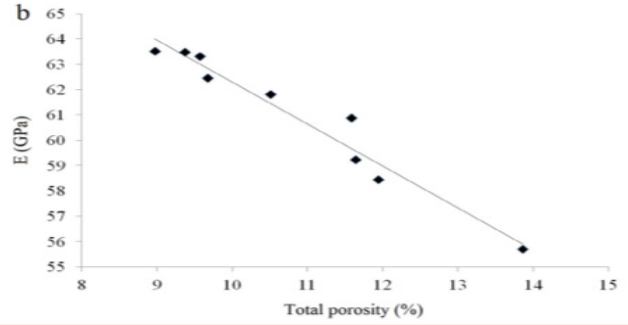

Figure 8b: The relationship between elastic modulus (E) values and total porosity.

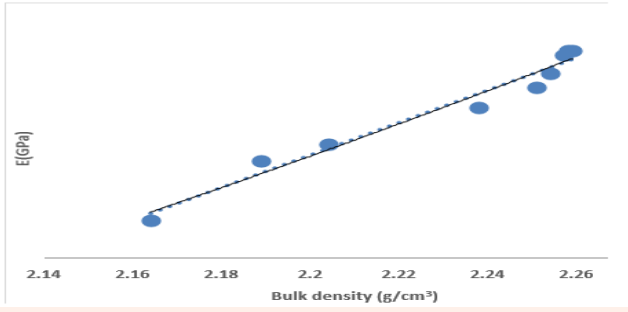

Figure 8c: The relationship between elastic modulus (E) values and the bulk density.

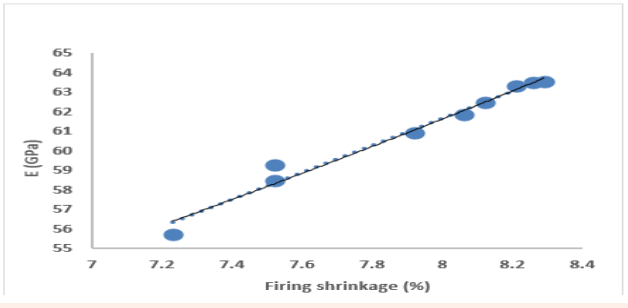

Figure 8d: The relationship between elastic modulus (E) values and the firing shrinkage.

Discussion

During firing, densification and shrinkage are firstly driven by the progressive melting of feldspars in combination with quartz and the heat transformed clays. At 1050–1100 oC, feldspar contributes strongly to the formation of a viscous flow, which is accompanied by the beginning of densification. Feldspar melting process is progressively changed by interactions with neighbouring fine quartz [43]. At the final sintering stage, when densification no longer vary, it is counterbalanced by the growing of new crystalline phases in the liquid phase (i.e. above 1250 oC). The predominant transformations are both the progressive nucleation and growing of mullite and the dissolution of quartz in the liquid phase. However, the composition of phases tends to reach equilibrium and the kinetic of transformation is very low. It also explains the decreasing of porosity and water absorption that attains the minimum value. These properties (mechanical strength, firing shrinkage, bulk density, water absorption and total porosity in porcelain) are closely related. An increase in temperature increases the densification by reducing the pores, which de- facto reduces the absorption of water [44]. Linear shrinkage and water absorption as essential parameters for establishing sintering curves are interdependent. Lower water absorption corresponds to greater linear shrinkage in the sintering process [45]. With a density value between 2.16 and 2.25; the estimated water absorbances are less than 0.5%, porosity less than 1.03% and the strength is above 50MPa. These results show that from this firing temperature, the formulated materials can be classified as porcelain. The glassy phases bind the grains thus leading to the cohesion of the material because they promote its densification and improves its mechanical properties. Firing above vitrification range results in a drastic fall of the physical properties due to forced expulsion of the entrapped gases resulting in blisters and bloating.

Conclusion

From the results presented, it is obvious that the investigations were successfully conducted. Three mineral raw materials from Nigeria used are suitable for the formulation of porcelain tiles. The abundance of raw materials makes the local production of porcelain in Nigeria economical and will stimulate the development of the country and earn foreign exchange for the nation.

References

1. Bergaya F, Lagaly G (2006) General introduction: clays, clay minerals, and clay science. In: Handbook of Clay Science, vol. 1 of Developments in Clay Science, Elsevier, Oxford, UK, pp. 1-18.
2. Ismail Y, Mikel DS, Robert JP (2009) Methods for purifying kaolin clays using reverse flotation, high brightness kaolin products, and uses thereof ceramic tiles-definitions, classification, characteristics and marking.
3. Sawadogo M, Zerbo L, Mohamed S, Sorgho B, Ouedraogo R (2014) Technological properties of raw clay based ceramic tiles: influence of talc. Sci Study Res 15: 231-238.
4. Romero M, Perez JM (2015) Relation between the microstructure and technological properties of porcelain stoneware. A Rev Mater Construc 65: 320. .
5. Sawadogo Y, Zebro L, Sawadogo M, Seynou M, Gomina M, et al. (2020) Characterization and use of raw materials from Burkina Faso in porcelain formulation. Results in Materials 6: 100085.
6. Boussak H, Chemani H, Serier A (2015) Characterization of porcelain tableware formulation containing bentonite clay. International Journal of Physical Sciences 10(1): 38-45.
7. Allessando F (2007) Thermal behaviour of the raw materials forming porcelain stoneware mixtures by combined optical and in-situ x-ray dila-tometry. AM Ceramic Soc 90(4): 1222-1231.
8. Mohamed S, Millogo Y, Ouedraogo R, Traore K, Tirlocq J (2011) Firing transformations and properties of tiles from a clay from Burkina Faso. Appl Clay Sci 51(4): 499-502.
9. Noni AD, Hotza D, Soler VC, Vilches ES (2010) Influence of composition on mechanical behaviour of porcelain tile. Part I: microstructural characterization and developed phases after firing. Mater Sci Eng 527: 1730-1735.
10. Yvon J, Lietard O, Cases JM, Delon JF (1982) Mineralogy of kaolin clays of charentes. Bull Miner 105 (5): 431-437.
11. Perez Jm, Rincon J, Romero M (2012) Effect of moulding pressure on microstructure and technological properties of porcelain stone ware. Ceram Int 38(1): 317-325.
12. Seynou ZL, Sorgho M, Lecomte-Nana B, Gomina G, Blanchart MP (2019) Microstructure and Weibull distribution of rupture strength of clay-talc ceramics. Ceramica 65: 240-245.
13. Fairhaust CW, Lockwood PE, Ringle RD, Thompson WO (1992) Effect of glaze on porcelain strength. Dent Mater 8(3): 203-207.
14. Radford KC, Lange FF (1978) Loading (L) factors for the biaxial flexure test. J Am Ceram Soc 61(5-6): 211-213.
15. Lamine Z (2014) Thermal transformations and structural reorganization of a clay. European Academics.
16. Martin Marquez J, Rincon JM, Remero M (2008) Effect of firing temperature on sintering of porcelain. Ceramic International 34(8): 1867-1873.
17. Marie NP (2015) Study of the microstructural transformations of clay/biomass mixtures during cooking and their relationship with mechanical and thermal properties. Thesis of the universite federale de Toulouse Midi-Pyrenees, France p. 53.
18. Garcia A, Aguilar-Elguezaba A (2009) Use of thermally treated bentonite clay in the formulation of ceramic tiles. Appl Clay Sci 46(3): 271-276.
19. Ayadi AJ, Soro J, Kamoun A, Baklouti S, Sfax RDS, Thomas AA (2013) Study of clay's mineralogy effect on rheological behavior of ceramic suspensions using an experimental design. Int J Res Rev Appl Sci 14(2): 374-384.
20. Kwak M, James DF, Klein K (2005) Flow behaviour of tailings paste for surface disposal. Int J Miner Process 77(3): 139-153.
21. Andreola F, Barbieri L, Corradi A, Lancellotti I, Manfredini T (2002) Utilization of municipal incinerator grate slag for manufacturing porcelainized stoneware tiles manufacturing. Journal of the European Ceramic Society 22(9-10): 1457-1462.
22. Hosseine MR, Seyed MS, Mohammad RA (2019) Biological separation of quartz from kaolin using *Baccillus Liecheniformis*. Separation Science and Technology 55(11).
23. Vasic MV, Pezo LL, Zdravkovic JD, Vrebalov M, RadojeviC Z (2018) Thermal, ceramic and technological properties of clays used in production of roofing tiles – principal component analysis. Sci Sinter 50: 487-500.
24. Yannick BI, Sylvain Ludovic WA, Francois N, Kabeyene K, Nathalie F (2019) Mineralogical transformation and microstructure of the alluvials clays. Sci Sinter 51(1): 57-70.
25. Martín-Marquez J, Rincon J, Romero M (2010) Mullite development on firing in porcelain stoneware bodies. J Eur Ceram Soc 30(7): 1599-1607.
26. Carbajal L, Rubio-Marcos F, Bengochea MA, Fernandez JF (2007) Properties related phase evolution in porcelain ceramics. J Eur Ceram Soc 27(13-15): 4065-4069.
27. Sainz MA, Serrano FJ, Amigo JM, Bastida JM, Caballero A (2000) XRD microstructural analysis of mullites obtained from kaolinite-alumina mixtures. J Eur Ceram Soc 20(4): 403-412.
28. Chen YF, Wang MC, Hon MH (2004) Phase transformation and growth of mullite in kaolin ceramics. J Eur Ceram Soc 24: 2389-2397.
29. Barlow SG, Manning DAC (1999) Influence of time and temperature on reactions and transformations of muscovite mica. Br Ceram Trans 98(3): 122-126.
30. Koffi LK, Joseph S, Siaka SN, Samuel O, Marie GJ, et al. (2006) Characterization of clay materials from the azaguie-blida site (anyama, ivory coast) and determination of the mechanical properties of ceramic products. J Soc West-Afr Chem 2: 35-43.
31. Osborn EF, Muan A (2006) Phase equilibria diagrams of oxide systems. The American Ceramic Society and the Edouard Orton, Ceramic Foundation, USA.
32. Gourouza M, Zanguina A, Natatou I, Boos Z (2013) Characterization of a mixed clay Niger. Rev Cames – Sciences Struct Mat.
33. Kozu S, Saikj S (2000) The thermal expansion of alkali-felspars. Sci Repts, Tohoku Imp Univ, Japan, 2: 203.
34. Maity S, Sarkar BK (1996) Development of high-strength whiteware bodies. Journal of the European Ceramic Society 16(10): 1083-1088.

35. Orts MJ, Escardino A, Amorós JL, Negre F (1993) Microstructural changes during the firing of stoneware floor tiles, Applied Clay Science 8 193-205.

36. Radomir S, Lucie K, Mukilas S (2017) The effect of different fluxing agent in the sintering of dry press porcelain bodies. Journal of Asian Ceramic Societies 5(3): 290-294.

37. Kingery WD (1976) Introduction to ceramics. J Wiley & Sons, New York, US.

38. Amorós JL, Cantavella V, Jarque JC, Felíu C (2008) Fracture properties of spray-dried powder compacts: effect of granule size. Journal of the European Ceramic Society 28(15): 2823-2834.

39. Revel GM (2007) Measurement of the apparent density of green ceramic tiles by a non-contact ultrasonic method. Exp Mech 47: 637-648.

40. Romagnoli M, Burani M, Tari G, Ferreira JMF (2007) A non-destructive method to assess delamination of ceramic tiles. J Eur Ceram Soc 27(1-3): 1631-1636.

41. Riley FL (2009) Structural ceramics. Fundamentals and Case Studies, Cambridge University Press, UK.

42. Rice RW (1998) Porosity of ceramics. Marcel Dekker Inc, New York.

43. Raimondo ZC, Dondi M, Guarini M, Tenorio Cavalcante GP (2004) Proc Qualicer I.

44. Siya M (2006) Nigerian Geological Survey Agency, Second Edition, Nigeria.

45. Chen Y, Zhang Y, Chen T, Liu T, Huang J (2013) Preparation and characterization of red porcelain tiles with hematite tailings. Construct Build Mater 38: 1083-1088.